symmetry

MDPI

Review

Symmetry and Electronic Properties of Metallic Nanoclusters

Emil Roduner [1,2]

[1] Institute of Physical Chemistry, University of Stuttgart, 70569 Stuttgart, Germany; e.roduner@ipc.uni-stuttgart.de
[2] Department of Chemistry, University of Pretoria, Pretoria 0002, South Africa

Abstract: Spherical nanoclusters with countable member atoms and delocalized valence orbitals are superatoms with properties analogous to those of simple atoms. This is reflected, in particular, in their optical spectra and magnetic properties, in a similar sense to transition metal ions and complexes. Clusters can be of low-spin or high-spin with considerable contributions to magnetism by the large cluster orbital magnetic moment. Due to the large radius of the clusters, they can be diamagnetic with an unusually high diamagnetic susceptibility. Gold and platinum, which in the bulk are non-magnetic, show pronounced superparamagnetism associated with their high-spin nature, and the magnetic moment can be trapped in symmetry-breaking environments so that hysteresis pertains far beyond room temperature. A significant deviation from hydrogen-like orbitals results from the shape of the confining potential, which has the effect that the orbital quantum number ℓ is not limited to values less than the principal quantum number n.

Keywords: superatom orbitals; nanocluster orbital moment; giant diamagnetism; high-temperature ferromagnetism; symmetry and countability of electrons; symmetry breaking in superatomic clusters

Citation: Roduner, E. Symmetry and Electronic Properties of Metallic Nanoclusters. *Symmetry* **2023**, *15*, 1491. https://doi.org/10.3390/sym15081491

Academic Editor: Valeriy Sbitnev

Received: 16 June 2023
Revised: 19 July 2023
Accepted: 25 July 2023
Published: 27 July 2023

1. Introduction

Nanoparticles are near-spherical or crystalline bodies with a relatively monodisperse size in the range of a few nanometers but not with an exact number of atoms. This distinguishes them from clusters which consist of a precise number of atoms arranged in structures which are often different from that of the bulk material. In particular, they may be of icosahedral symmetry, which has five-fold rotation axes that are not compatible with translational symmetry of traditional crystals and occurs only in quasicrystals. The type of atoms, their structure and morphology, as well as the nature and stoichiometry of protecting capping agents or of a confining porous host material have a pronounced impact on their physical and chemical properties. In the present case, it is the aspect of symmetry which is of interest. High symmetry excludes many of the possible morphologies and restricts the choice to near-globular clusters. A second constraint comes from the viewpoint of interaction between the atoms. Noble gas clusters are weakly bound by dispersion interactions which do not much alter the properties in the cluster from those of the free atoms. Ionic clusters which are strongly bound have properties similar to those of the bulk salt. These two cases have in common that each electron is mainly localized on a single atom. Of interest here are the intermediate cases of covalent bonds where the valence electrons are delocalized over the entire cluster, giving them pronounced size-dependent properties [1]. In the absence of a gap within the highest occupied band, these systems are dubbed metals, and those in the presence of a gap of up to a few eV between the valence and conduction band are called semiconductors.

The nice property of truly spherical systems is that this allows the separation of the radial from the angular coordinates in quantum chemical calculations involving the delocalized electrons. Even though this is a gross simplification because it neglects the important electron–electron interaction, also called electron correlation, it has the nice effect that the energies depend only on the radial part of the wavefunction, and it leads

to the degeneracy of all electrons which belong to the same principle quantum number n. Electron correlation lifts the degeneracy of orbitals with different values of the orbital angular momentum ℓ, retaining for spherical symmetry a $2\ell + 1$ degeneracy according to the values of the magnetic quantum number m_ℓ. When spherical symmetry is broken, this degeneracy is also lowered or completely lost. In complete analogy to atoms, degeneracy of energy levels in clusters also reflects their symmetry. Molecular orbitals of spherical clusters mimic the properties of atoms; they are, therefore, called superatoms or pseudoatoms [2,3]. What has mostly been ignored so far in literature is the fact that also cluster orbitals possess an angular momentum ℓ. As for atoms, orbitals with different ℓ but identical n are no longer degenerate due to different degrees of shielding.

The superatomic core can consist of a single element, or it can be an alloy, as long as an atomic orbital symmetry is retained. For example, the central atom of a small icosahedral cluster can be a different element and serve to tune the electron count to complete or purposely incomplete shells. Charge distributions are similar to those of semiconductor core–shell nanoparticle structures, and their effect for chemical interactions is well understood [4].

In analogy to atoms, superatoms can also react with each other and form dimers or linear trimers of $Pt@Ag_{12}$ units [5–8].

The trimer is isolobal of the linear tri-iodide anion, I_3^-, which lowers the symmetry to axial [9–12].

2. Superatom Properties

Accurate quantum chemical calculations of heavy metal clusters are relatively time-consuming. However, a simplified model, called the Jellium model, in which the explicit Coulomb potentials of the electrons are replaced by a phenomenological confining potential and the atomic cores by a structureless background provide a qualitative understanding. Figure 1 shows one-electron energy levels for three radial dependences of different shapes of a confining potential. A large cluster comes closest to the spherical box potential that has a flat bottom (right entry), while the 3D harmonic oscillator model (left entry) reproduces better a very small cluster because it does not have a flat range at the bottom. Hydrogen-like atoms with a single nucleus exhibit the familiar $-1/r$ Coulomb potential with a negative infinity cusp and are not shown. Small spherical clusters follow best the intermediate case represented by the rounded box. Importantly, the shape of the potential has a pronounced effect on the periodicity of the energy levels. For the harmonic oscillator they are proportional to n and, therefore, equidistant. For the hydrogen atom with the negative cusp, the levels close up at high energies, scaling with $1/n^2$, and the density of states approaches infinity towards the dissociation level at $E = 0$, whereas they scale with n^2 for the square well potential.

From the well-known hydrogen atom wave function, we have the s, p, d, f, g ... subshells given by the restriction of orbital angular momentum quantum number $\ell < n$. For the phenomenological potentials $V \neq -1/r$, this restriction to $\ell < n$ does no longer hold, and all values of ℓ are possible for each principal quantum number n [13].

The selection rules for optical electric dipole transitions are entirely based on the symmetry of the angular wavefunctions, and they are thus the same as for the hydrogen atom, where we have $\Delta\ell = \pm 1$ as a consequence of the photon angular momentum $\ell = 1$ and angular momentum conservation. There is no constraint on Δn, but for 3D problems there is a third quantum number m_ℓ, the magnetic quantum number, with $|m_\ell| \leq \ell$, for which the selection rule is $\Delta m_\ell = 0, \pm 1$. Of course, the final state of a transition must be incompletely occupied in order to accommodate the promoted electron.

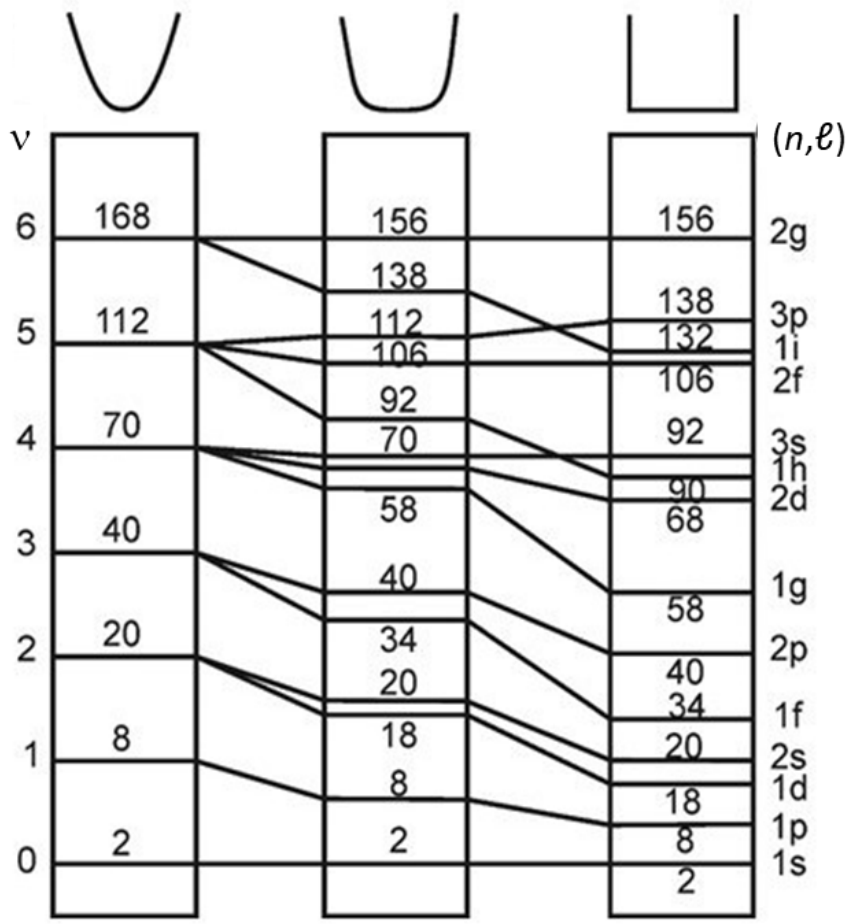

Figure 1. One-electron energy level scheme for phenomenological confining 3D quantum well potentials of parabolic, rounded square and purely square well shape. The numbers give the electron occupancy added up from the ground state. The energy level structure is solely given by the shape of the potential and thus by the radial wave function. Reprinted with permission from ref. [13]. Copyright (2004) by the American Physical Society.

The superatom concept has been defined clearly by Walter et al. [2]. At first, this concept ignores all core electrons of the undelaying noble gas configuration. The valence electrons are then treated according to the Jellium model with an Aufbau rule following Figure 1 for delocalized superatomic electrons, giving orbitals typically in the angular momentum sequence $1S^2$ | $1P^6$ | $1D^{10}$ | $2S^2$ $1F^{14}$ | $2P^6$ $1G^{18}$ | $2D^{10}$ $3S^2$ $1H^{22}$ |. For medium size gold clusters, exceptional stability is found for a total count of n^* = 2, 8, 18, 34, 58, 92, 138... metallic valence electrons, depending somewhat on the mean field confining potential [2]. These numbers form secondary closed shell configurations above the noble gas cores. Only the electrons above the highest possible closed shell electron count are relevant for the superatomic orbitals of interest, since after a correction for the net charge of a cluster and a second correction for the contribution of the electron withdrawing or electron donating ligands, they determine the spectroscopic, magnetic, and chemical properties [2]. In particular, for the magnetic properties, the exact count of these remaining valence electrons is crucial.

In real clusters, the valence electrons are confined by the Coulomb potential of the positive atomic cores. This imposes a structure on the results of the Jellium model. There is no analytical solution for the wavefunctions of such systems, but the result of ab initio density functional calculations at the B3LYP/LANL2DZ level for the molecular orbitals of the icosahedral core–shell cluster $A\ell Pb_{12}^+$ serves as an instructive example because it shows the compelling analogy of the symmetry of molecular orbitals with the familiar H atom orbitals (Figure 2) [14].

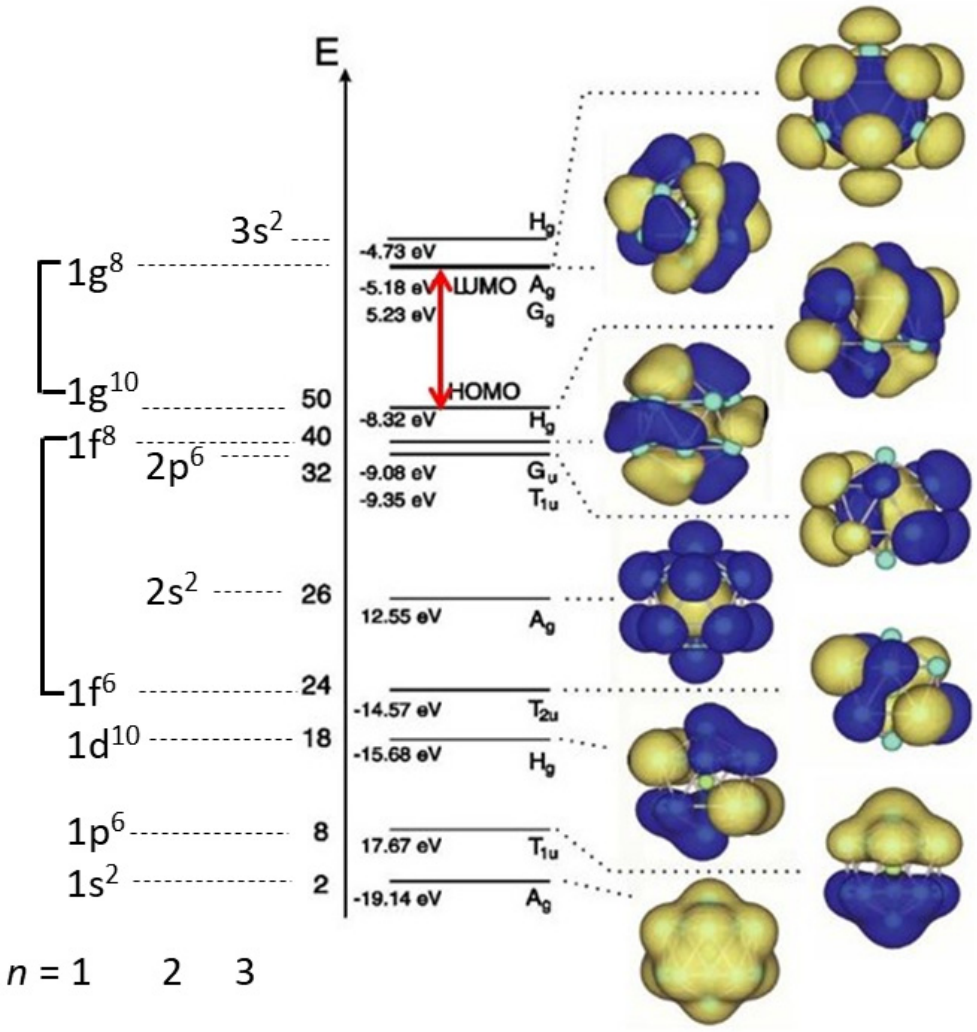

Figure 2. Calculated electronic orbitals (one for each set) for the core–shell icosahedral cluster $A\ell Pb_{12}^+$. The overall cluster molecular orbitals resemble the spherical harmonics of atomic orbitals. On this ground, small clusters are often called 'superatoms' or 'pseudoatoms'. Adapted from ref. [14] Copyright (2004) by the American Physical Society.

However, the isoelectronic surface of the s orbitals is not a smooth sphere; the surface reflects the structure of the lead atoms underneath. As expected, 2s orbitals have one and 3s orbitals two near–spherical nodal surfaces. p, d, and f orbitals show the expected nodal planes through the center. The highest symmetry element of the icosahedral $A\ell Pb_{12}^+$ (I_h symmetry) are six five-fold rotation axes; the highest degeneracy of orbitals is thus limited to five. This is seen for the 1f orbitals, which in spherical symmetry would require a seven-fold degeneracy that cannot be accommodated. Therefore, this set of orbitals splits into two sets, one of $1f^6$ and one of $1f^8$ occupancy. For the same reason, the set of $1g^{18}$ orbitals splits into two sets, represented by $1g^{10}$ and $1g^8$ configurations, allowing for a pronounced HOMO-LUMO energy gap of 3.1 eV (red arrow in Figure 2) [14].

$A\ell Pb_{12}^+$ has 50 valence electrons, therefore, all subshells up to the $1g^{10}$ orbital are fully occupied and the system is diamagnetic with no net orbital momentum.

3. Energy Splitting by Symmetry Breaking Due to Cluster Environment

The similarity with atomic orbitals allows us to explore possible consequences in analogy to superatomic orbitals. A well-investigated effect is that of symmetry breaking due to the interaction of d orbitals with ligands in solution (ligand field effect) or with the crystal field in solids (crystal field effect) as demonstrated in Figure 3. The five dorbitals of

a free transition metal ions are energy-degenerate. The environment leads to symmetry-compatible splitting patterns, and the size of the splitting increases with the strength of the interaction.

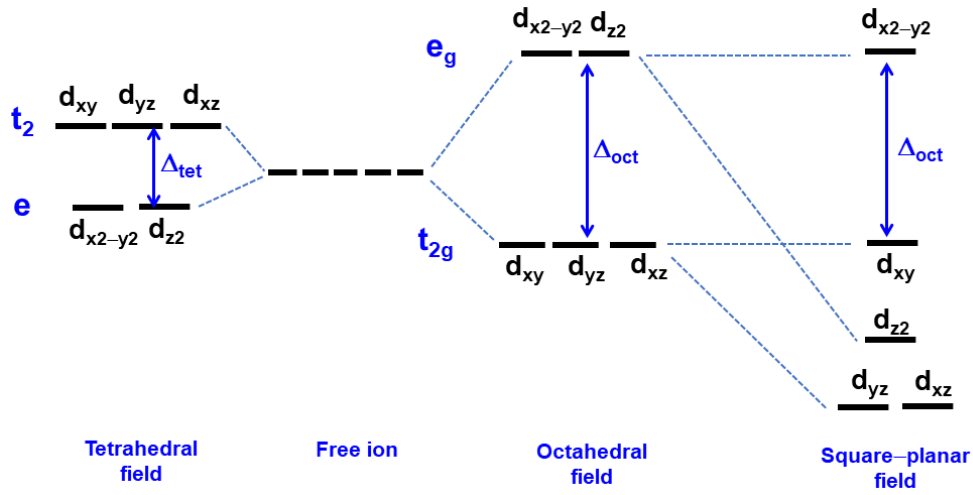

Figure 3. Crystal field effect of d orbitals with ligands in environments of different symmetries.

Interactions which give a bonding effect of any kind will lower the energy of the d orbital, while an antibonding interaction, e.g., of a ligand lone pair with an occupied d orbital will raise its energy. The effect is that a tetrahedral field splits the d orbitals into a doubly and a triply degenerate set of energy levels, with the triplet being of a higher energy. For an octahedral field, one also finds two sets, but with the opposite energetic effect. A square-planar field represents the lowest symmetry which thus leads to a more complex pattern with the highest degeneracy being two-fold.

The effect of splitting becomes apparent in UV-Vis absorption spectroscopy. In principle, transitions within the d manifold are Laporte forbidden because of $\Delta\ell = 0$. However, in a slightly broken symmetry with split energy levels, this transition becomes weakly allowed and leads to faint absorption bands which are used to analyze the local symmetry.

More important is the effect on the magnetic structure. Let us assume that we have a central d orbital with three electrons. For the free ion and for the octahedral field, we then have all three electrons unpaired. This may be different for the tetrahedral coordination. If the ligand interaction is weak and the energy splitting Δ_{tet}, therefore, is small, all three electrons will still be unpaired, which is a high-spin configuration. However, when the interaction exceeds the spin pairing energy, the third electron will relax to the lowest state, leaving us with a single unpaired electron low-spin configuration.

The picture of Figure 3 with degenerate energy levels is susceptible to complications. The Jahn–Teller theorem states that all non-linear molecular systems with a partly occupied degenerate electronic state are unstable and relax their energy by spontaneously lowering their symmetry and thereby reducing the energy degeneracy [15].

It is straightforward to extrapolate the situation to clusters. Free, bare clusters can be prepared and studied from molecular beams and upon condensation in atomic beams with mass-spectrometric characterization as described elsewhere [13]. In condensed phases, clusters are often reactive and need protection from agglomeration. This can be done by embedding them in polymers or in zeolite pores, or by capping them with a shell of protecting ligands. Interaction with these protecting agents often breaks the symmetry and affects the frontier energy levels.

A highly symmetrical near spherical or icosahedral free superatom gets axially distorted when the cluster sits inside a sufficiently narrow cylindrical pore or when it simply sits on the surface of a support. This breaks the symmetry of the cluster and reduces the degree of degeneracy of the relevant orbitals. The result may be a highly susceptible magnetic behavior, as we will see further below.

4. Cluster Orbital Angular Momentum and Spin–Orbit Coupling

Figure 2 shows the orbitals in the real representation which do not possess an angular momentum (e.g., the real linear combinations p_x and p_y in place of the original but equivalent complex p_+ and p_-). However, we know from the hydrogen atom that orbitals with quantum number $\ell \neq 0$ do have an angular momentum. Classically, this is represented by a current I on a circle with radius r and enclosed area A, which leads to a magnetic moment μ [16]:

$$\mu = I \cdot A = \frac{qv}{2\pi r} \times \pi r^2 = \frac{q}{2m_e} \times m_e v r = \frac{q}{2m_e} L, \quad (1)$$

where q is the electron charge, m_e its mass, v its velocity, and L the angular momentum. For equal velocities, the magnetic moment scales with $A = \pi r^2$, revealing an enormous enhancement of the magnetic moment due to the larger radius of a superatom compared with a normal atom.

The orbital angular momentum of a subshell is obtained by adding up the m_ℓ values of all its electrons. Due to occupation according to Hund's rules, this causes half-filled and completed shells to have zero orbital momentum, i.e., these shells have full spherical symmetry. Independently, there is of course an electron spin angular momentum, which is non-zero for a half-filled shell. However, the greatly complicating effect of spin–orbit coupling occurs only when both angular momenta are non-zero. For optical transitions from filled or half-filled shells the final (excited) state will be affected [17]. We agree that the band splitting in the optical transition is due to spin–orbit coupling, but note that the fully occupied HOMO ground state given in Figure 5 of [17] has zero orbital and zero spin moment, so there can be no spin orbit coupling, while it is fully plausible that this effect occurs in the excited state with both the orbital and spin moment being non-zero.

A large orbital angular momentum can be trapped along an axial distortion from the environment, leading to hysteresis of magnetization in a magnetic field.

5. Coexistence of Various Magnetic Properties of $Pt_{13}H_x$ in Zeolite Pores

Monodisperse platinum nanoclusters can be synthesized in the pores of zeolites via exchange of the sodium cations by $Pt(NH_3)_4Cl_2$ salt followed by hydrogen reduction (Figure 4a). Extended X-ray absorption fine structure (EXAFS) analysis shows their structure to be icosahedral with 13 ± 2 atoms which occupy 1 of every 25 pores of NaY zeolite [18]. Maximum hydrogen coverage corresponding to $Pt_{13}H_{38}$ was determined [19], which is more than 3 H for each of the 12 surface Pt atoms. For bulk crystalline Pt, a value of 1 H per Pt is normally assumed and used to determine the surface of Pt catalysts. The preferred binding sites of H on Pt(111) surfaces is the three-fold hollow site. The 36 H atoms can bind to the edge and corner sites of icosahedral clusters, and the edge site that bridges two Pt atoms was indeed confirmed from IR spectroscopy to be the main binding site [20]. H can be reversibly adsorbed and desorbed or exchanged with D [21].

While platinum is diamagnetic in the bulk, a fraction of 10–20% of these clusters show a pronounced superparamagnetism that depend on the extent of hydrogen coverage; about 0.03% is EPR active, and the major fraction is diamagnetic. If all clusters have the same structure, why then is there a coexistence of different forms of magnetism? The answer is that zeolites, although they are perfectly crystalline, are heterogeneous. The negatively charged aluminum ions substitute silicon randomly at its tetrahedral lattice sites, under the constraint of the Loewenstein rule which does not allow two aluminum ions separated by only one oxygen bridge. This has the consequence that not all pores are equally charged (or charge balanced by a proton) and even equal charges may be differently distributed, which may also slightly break the symmetry. It is furthermore not known whether the clusters are all electrically neutral or whether they assume a residual positive or negative charge.

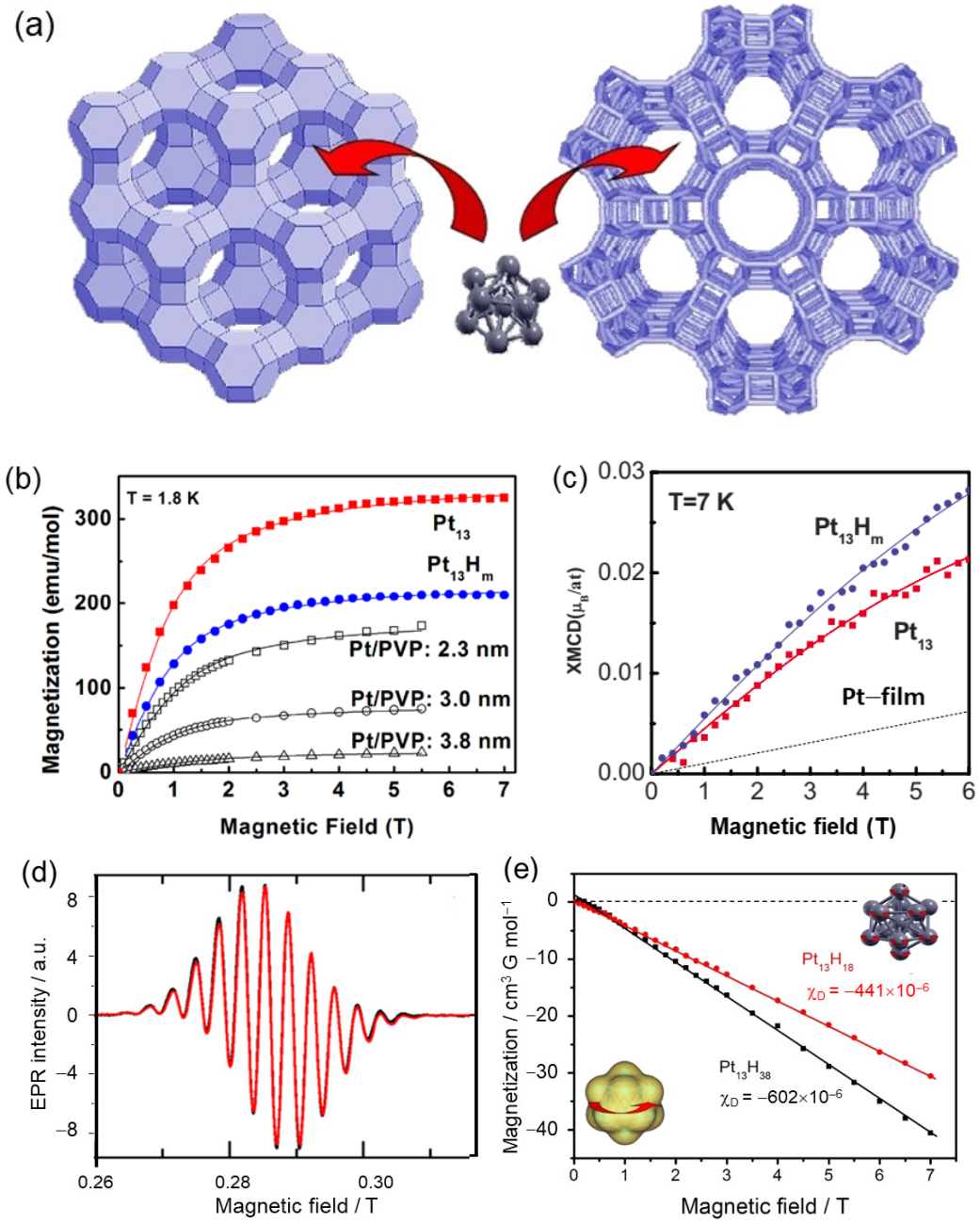

Figure 4. (**a**) Icosahedral 13-atom Pt cluster to scale with porous supports cubic NaY zeolite (**left**) and KL zeolite (**right**) that has one-dimensional pores. (**b**) SQUID magnetization measurements of Pt nanoparticles in polyvinylpyrrolidone (PVP) [21] polymer and hydrogen-covered and desorbed Pt_{13} nanoclusters in NaY zeolite. (**c**) XMCD measurements of hydrogen-covered and desorbed Pt_{13} clusters in NaY zeolite, in comparison with Pt foil (reprinted with permission from ref. [22]). (**d**) EPR spectrum of paramagnetic hydrogen-covered $Pt_{13}D_m$ clusters in KL zeolite at 4 K with superimposed simulation (m not exactly determined) [21,23]. (**e**) SQUID magnetization measurements of Pt_{13} nanoclusters at two hydrogen coverages at 295 K [24]. (**a**,**b**,**d**) Reprinted from ref. [21] (https://creativecommons.org/licenses/by/4.0/, accessed on 10 June 2023).

It has been known for some time that gold and platinum nanoparticles protected in polyvinylpyrrolidone (PVP) polymer show size-dependent magnetism that increases with decreasing size (Figure 4b), suggesting that it is a surface effect [25,26].

Measurements of the magnetization M as a function of the applied magnetic field H can be obtained using a Superconducting Quantum Interference Device (SQUID) or X-ray

magnetic circular dichroism (XMCD). At low temperature, this yields a Langevin-type curve as shown in Figure 4b,c:

$$M(H) = fN_A \frac{\mu}{13}\left[\coth\left(\frac{\mu H}{k_B T}\right) - \frac{k_B T}{\mu H}\right] + \chi_0 H \quad (2)$$

where μ is the magnetic moment of the cluster (in Bohr magnetons, μ_B) which represents a fraction f of all Pt atoms in the sample, k_B is the Boltzmann constant, T the temperature, and χ_0 a temperature-independent magnetic susceptibility [21]. The total magnetization is given by the saturation level of $M(H)$, while the magnetic moment is obtained from the initial slope that displays good Curie behavior. The curves show no hysteresis, revealing a super-paramagnetic state. The SQUID measurements have to be corrected for the empty zeolite because of possible iron impurities. The XMCD method is element-specific and has the further advantage that it can distinguish between the spin and the orbital moments, while the SQUID data contain both contributions (Table 1).

Table 1. Magnetization parameters μ for high-spin platinum clusters in NaY, their fractions f, and the average atomic spin and orbital magnetic moments m_S and $m_{L.}$ (Reprinted from ref. [21] (https://creativecommons.org/licenses/by/4.0/, accessed on 10 June 2023).

Property	SQUID Measurements, 1.8 K		XMCD Measurements, 7 K		
	Pt_{13}	$Pt_{13}H_m$	Pt_{13}	$Pt_{13}H_m$	Pt Foil
μ/μ_B per Pt_{13}	5.9(1)	5.6(1)	3.7(4)	3.0(4)	--
f/%	14(1)	10(1)	14(10)	20(10)	--
10^3 m_L/μ_B per Pt	--	--	5.49(9)	6.39(7)	2.1(1)
10^3 m_S/μ_B per Pt	--	--	17.1(6)	21.8(6)	5.5(1)
m_L/m_S	--	--	0.32(2)	0.29(2)	0.38(2)

Interestingly, the results of XMCD in Table 1 reveal that the orbital moment m_L per atom is larger for the clusters by about a factor 3 compared with the Pt foil, whereas the spin moment m_S is larger by a factor 3–4, depending slightly on the amount of adsorbed H. This demonstrates that the cluster structure warrants a considerably larger number of unpaired electrons compared to the bulk metal. The number of unpaired spins in a non-magnetic bulk metal is generally low, and the dependence on the electronic structure of the clusters and their hydrogen coverage is explained schematically below in Figure 5. The SQUID and the XMCD data per Pt_{13} show qualitatively consistency but not quantitative agreement, probably indicating limitations in reproducibility of sample handling. In all cases, the cluster orbital moment contributes about one-third in addition to the spin moment, which explains part of the difference.

The cluster leads to an impressive near-isotropic multiplet in EPR spectroscopy at 4 K. In Figure 4d, we show the deuterium exchanged cluster because of the much better resolution due to the much smaller nuclear magnetic moment of D relative to H, which reveals that the hydrogen hyperfine coupling is not resolved but affects the linewidth. The spectrum is quantitatively simulated, assuming an electron spin-1/2-system that interacts with 12 Pt nuclei and accounting for the proper distribution of all possible isotopic compositions (38.8% with nuclear spin-1/2, all other isotopes with nuclear spin zero) [23]. There is no resolved splitting of the central Pt nucleus, which is compatible with a symmetry of the cluster wavefunction that has a node at the central atom (no s character). The simulation reveals an isotropic Pt hyperfine coupling of 6.81 mT, but a small axial anisotropy of the electron g value, reflecting a slight distortion of the cluster in the cylindrical pore of the KL zeolite but notably also in NaY with its spherical cavities, even though the hydrogenated clusters do not quite fill the available space in the pores. In principle, the anisotropy could represent a Jahn–Teller effect in which the singly occupied orbital gains energy by reducing its symmetry, but this aspect has not yet been further investigated. g_{so} ranges between 2.367 and 2.378, depending on hydrogen coverage. This value is considerably higher than

g_e, which for atomic d orbitals is an indication that the unpaired electron relates to a hole in a more than half-filled d-shell [27]; this interpretation may also hold for the cluster orbitals. The same spectrum is seen at coverages between 5 and 30 D per cluster, with an intensity that increases near-linearly with deuterium coverages (Figure 3b of ref. [23]).

An advanced pulsed magnetic resonance technique, called hyperfine sublevel correlation experiments (HYSCORE), can resolve two types of hydrogen with different hyperfine couplings of axial symmetry, one with a larger coupling that saturates at a coverage of 12 H per cluster and may, therefore, belong to H bound atop of atoms, while the other one increases in amplitude up to a coverage of 38 H [23].

We have already seen in Figure 4b that the saturation magnetization also depends on hydrogen coverage. In order to understand this behavior, we have drawn a schematic level diagram for the clusters. Platinum has the electron configuration [Xe]$4f^{14}5d^{9}6s^{1}$. The 4f are energetically lower by 73 eV than the 5d and 6s electrons and have an atomic $<r^2>$ expectation value of only 0.3 $a_0{}^2$, an order of magnitude less than the 4d electrons [28]. We, therefore, count them as part of the undelocalized atomic core. Thus, only the 130 5d and 6s electrons of the 13 Pt atoms contribute to the delocalized superatomic orbitals. The appropriate Aufbau rule of delocalized superatomic orbitals of metal clusters is $1S^2\ 1P^6\ 1D^{10}\ 2S^2\ 1F^{14}\ 2P^6\ 1G^{18}\ 2D^{10}\ 3S^2\ 1H^{22}$ . . ., wherein S–P–D–F–G–H denote the angular-momentum characters [2], which is compatible with the Jellium model level schemes. They accommodate 92 electrons and represent a superatomic core, leaving 130 − 92 = 38 electrons to be involved as superatomic valence electrons in the bonding of surface-adsorbed hydrogen. This matches nicely the saturation coverage of 38 H per cluster, suggesting that coverage saturation is determined primarily by the number of available electrons rather than to specific and not very selective bonding sites at the surface. On this basis, we have drawn an energy level scheme (Figure 5), based on numerical values reported by Watari and Ohnishi [29]. Considering that quantum chemical calculations of heavy atoms have limited accuracy, that the clusters are located in a somewhat heterogeneous environment, and that we are not even sure about the charge neutrality of the clusters, we stress that this is not a quantitative, but only a schematic representation that allows a qualitative discussion of the observed coverage behavior.

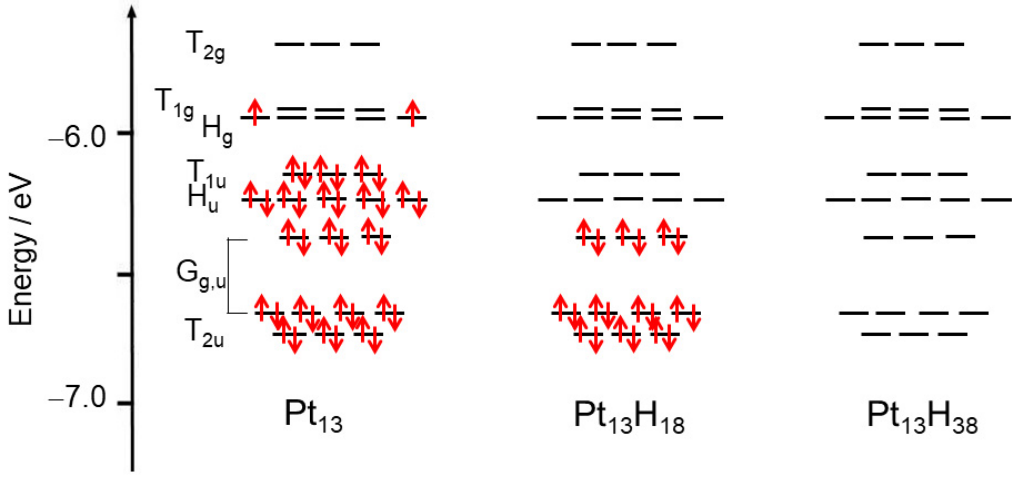

Figure 5. Schematic representation of level occupancy of differently hydrogen–covered Pt_{13} clusters. Red arrows represent electron spins up and down. Level structure taken from ref. [29].

The first entry is for the hydrogen desorbed neutral Pt_{13} cluster and shows all 38 superconductive valence electrons. The figure shows an assumed case of two unpaired electrons, but according to Table 1, this should probably be about five. Adsorption of each hydrogen atom binds one of these electrons under formation of a hydride-like species that is ca. 5 eV below the Fermi level [30] and, therefore, significantly off-scale in Figure 5. The important fact is that each additional surface hydrogen changes the magnetic state of the

cluster by "titrating out" the electrons one-by-one, which leads to oscillations as a function of hydrogen coverage. Such behavior was indeed observed [23], but equilibrium seemed to partly adapt on a timescale of months only. Overall, traditional magnetic materials achieve a magnetization that corresponds up to a few unpaired electrons per atom, while the clusters provide a limited level degeneracy that can only accommodate a few unpaired electrons per cluster.

A novel and intriguing form of magnetism, called giant diamagnetism, is displayed in Figure 4e. It is present at all temperatures and in all clusters, but because it is still weak compared with the other forms of magnetism, it is detected best at room temperature or above when superparamagnetism has damped out. On the ground, that diamagnetism of materials is due to ring currents induced on atoms by an applied magnetic field; it can be predicted to a good approximation by adding up tabulated atomic increments. The induced magnetic moment is antiparallel to the applied field, scales linearly with field, and the diamagnetic susceptibility is obtained from the slope of the linear behavior. Our observations shown in Figure 4e do show this behavior, except that the slope is larger than expected based on tabulated values by a factor 37–50, and it depends on hydrogen coverage [24]. This behavior was even predicted for sodium nanoclusters before its first observation with platinum. [31]. For the Pt clusters, it is near-quantitatively explained in terms of ring currents on the clusters where the magnetic moment scales with the area of the enclosed rings (Equation (1)). It was also observed for Cu nanoclusters [32].

6. Magnetism of Gold Nanoparticles and of Ligand-Protected Gold Clusters

Several forms of magnetism were also observed and discussed for gold nanoparticles [33]. As for Pt, there is size-dependent superparamagnetism. What looks like a smooth size-dependence for the limited data in Figure 4b for Pt is not reproduced and looks rather erratic for gold nanoparticles (Figure 6a) [33] and reminds more of the variations observed with hydrogen coverage of Pt_{13} [23]. The behavior is consistent with a changing symmetry related to frontier orbital degeneracy and electron occupation with size and is similar to the hydrogen coverage effect shown in Figure 5. The reason for the debated lack of reproducibility is to be sought in the variation of electron counts in the superatomic shell, which in part rests on the lack of atom-precise control of the nanoparticle size.

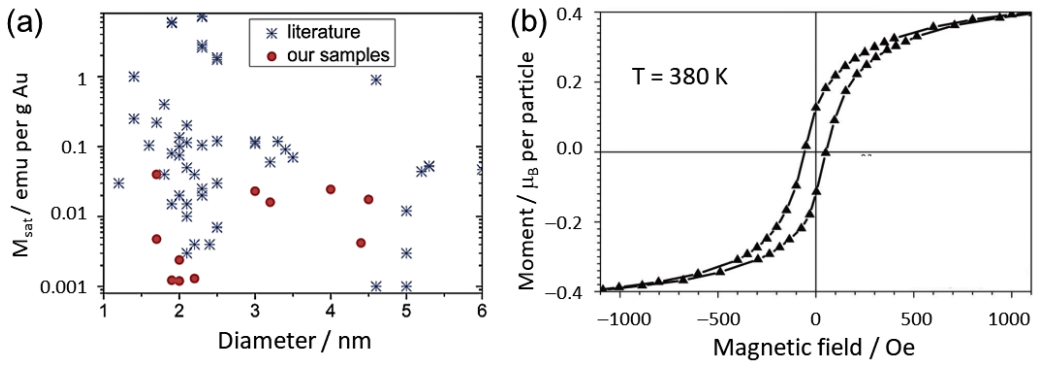

Figure 6. (**a**) Size dependence of saturation magnetization of Au nanoparticles. (**b**) Magnetization hysteresis loop of a 2.1 nm Au nanoparticle at 380 K. Reprinted with permission from ref. [33].

A remarkable finding is the observation of magnetic hysteresis curves at temperatures as high as 380 K. This is the behavior expected for long-range ordered ferromagnetic materials, or for superparamagnetic systems below the blocking temperature. A 2.1 nm particle is not a long-range coupled spin system, and it is not a cluster with a countable number of atoms. Spins in superparamagnetic systems can normally easily reorient since the blocking temperatures are typically much below 100 K. In the spirit of Figure 3, there must thus be an interaction that locks the spin to the environment. This can be the cluster or nanoparticle orbital moment as we have seen that it depends on the anisotropy of the crystal

field of the surrounding. The existence of a high-temperature hysteresis is good evidence for the presence of an orbital angular momentum. It should be noted that the relatively weak signal represents an unknown but small fraction of the total gold in the sample.

In agreement with results for the Pt_{13} clusters, there is an enhanced diamagnetism, with a size-dependent diamagnetic susceptibility per gram that is larger for the 3.5 nm than for the 2.2 nm nanoparticles. It is compatible with the ring current interpretation that it increases with cluster size, but it should be expected that this trend should pass a maximum before it decreases towards the bulk value.

A systematic view of ligand-protected gold cluster superatom complexes has been developed by Walter et al. on the basis of density functional calculations [2]. The geometric and electronic structures of complexes with 11, 13, 39, and 102 gold atoms capped with thiolate, phosphate, and halide ions were analyzed, and their extra stability with a pronounced HOMO-LUMO gap was related to superatomic noble-gas-like closed shell configurations according to the Aufbau rule mentioned above in context with Figure 5. The electron count has to take into account the ionic charge of the gold core in context with electrons transferred to the ligands.

The $Au_{25}(SR)_{18}^{-}$ thiolate cluster has been dubbed the "poster child" of success in applying the superatom complex concept and remains the most studied system of this kind [17]. The origin of a mysterious doublet in the UV-Vis transition from the filled triply degenerate HOMO p-shell to the empty LUMO shell was clarified in two-component density functional calculations by inclusion of spin orbit coupling which led to splitting of the excited state by about 0.20 eV, an effect that is familiar from transitions involving conventional atomic orbitals. This confirmed the existence and importance of orbital angular momenta in superatomic orbitals.

7. Conclusions and Outlook

The superatom concept is a useful model that describes adequately the properties of high symmetry nanoclusters with delocalized electrons. For the interpretation, it is crucial to know the precise number of electrons, which requires a uniform stoichiometry and structure of the clusters in the sample. A variability of the atom count, as it is common for nanoparticles, leads to a distribution of properties and often to irreproducible results, in particular with respect to magnetism. Low-spin and high-spin superparamagnetic states and the influence of symmetry reduction by interaction with the environment are understood by analogy to crystal field theory for transition metal ions.

The cluster orbital moment is large because it scales roughly with the square of the cluster radius. It adds to the spin moment and contributes significantly to the total magnetic moment. Its orientation can be trapped by the environment, which may cause magnetic hysteresis up to high temperatures without the need of any long-range interaction. Independent of any spin-related magnetism, clusters and also nanoparticles reveal spectacular values of diamagnetic susceptibility with increasing size.

The superatom concept has been applied mainly to gold and platinum clusters and to a few other systems. However, it could be extended to a large variety of other metallic systems. For example, it has been predicted theoretically and verified experimentally without resorting to the superatom interpretation that free clusters of nonmagnetic elements, such as Ti, V, Rh, and Pd can become magnetic, whereas the magnetic moments per atom of Fe, Co, and Ni clusters exceed their respective values in the bulk phase [34]. The magnetic moment of neutral Fe_{13} clusters was determined experimentally to be 34 μ_B, or 2.9 μ_B per atom and from theoretical calculations as much as 44 μ_B for the ground state (3.4 μ_B per atom, not including the orbital momentum) [34], which is significantly more than the bulk value of 2.2 μ_B per atom. It would be interesting to study the ferromagnetic or antiferromagnetic coupling behavior within arrays of clusters.

An interesting superatom case is the Al_{13} cluster that has 39 valence electrons and, therefore, tends to accept an electron to complete a noble-gas-like atomic shell of 40 electrons in the Jellium model (Figure 1). It thus simulates a halogen atom, and in $Al_{13}I$ the cluster

is the anion and iodine is the cation, which is the opposite of the common behavior of atoms [35].

Zeolites are attractive hosts for clusters and have been investigated in particular in view of catalysis. Based on the giant diamagnetism of $Pt_{13}H_x$ clusters for NaY samples in which only one in 25 cages was occupied with a cluster, it was suggested that a higher loading of clusters might lead to superconductivity at room temperature [24]. Hydrides are suggested in general as promising candidates for high temperature superconductivity [36]. Metal clusters with 10^2–10^3 free carriers in superatoms may exhibit strong superconductive pairing accompanied with the appearance of orbital diamagnetism below T_c [37]. The conditions remind strongly of the observations reported in Figure 4d and suggest that a higher loading of Pt clusters, which satisfy the condition with 130 free carriers, should be synthesized in order to satisfy the conditions for room temperature superconductivity.

Funding: This research received no external funding.

Conflicts of Interest: The author declares no conflict of interest.

References

1. Roduner, E. Size matters: Why nanomaterials are different. *Chem. Soc. Rev.* **2006**, *35*, 583–592. [CrossRef]
2. Walter, M.; Akola, J.; Lopez-Acevedo, O.; Jadzinsky, P.D.; Calero, G.; Ackerson, C.J.; Whetten, R.L.; Grönbeck, H.; Häkkinen, H. A unified view of ligand-protected gold clusters as superatom complexes. *Proc. Nalt. Acad. Sci. USA* **2008**, *105*, 9157–9162. [CrossRef]
3. Roduner, E. Superatom Chemistry: Promising Properties of Near-Spherical Noble Metal Clusters. *Phys. Chem. Chem. Phys.* **2018**, *20*, 23812–23826.
4. Roduner, E.; Krüger, T.; Forbes, P.; Kress, C. *Optical Spectroscopy—Fundamentals and Advanced Applications*; World Scientific: London, UK, 2019; Chapter 5.
5. Kang, X.; Xiong, L.; Wang, S.; Pei, Y.; Zhu, M. De-assembly of assembled Pt_1Ag_{12} units: Tailoring the photoluminescence of atomically precise nanoclusters. *Chem. Comm.* **2017**, *53*, 12564–12567. [CrossRef] [PubMed]
6. Miyajima, S.; Hossain, S.; Ikeda, A.; Kosaka, T.; Kawawaki, T.; Niihori, Y.; Iwasa, T.; Taketsugu, T.; Negishi, Y. Key factors for connecting silver-based icosahedral superatoms by vertex sharing. *Nat. Commun. Chem.* **2023**, *6*, 57. [CrossRef]
7. Zhang, Y.; Li, X.; Lu, J.; Li, S.; Zhang, Y. Endohedral group-14 clusters $Au@X_{12}$ (X = Ge, Sn, Pb) and their anions: A first-principles study. *J. Molec. Liquids* **2023**, *376*, 121477.
8. Nishimura, T.; Toba, T.; Sakane, G.; Ishii, T. Periodicity of Superatomic Hybrid Orbitals in Substituted Superatoms and Superatomic-like X@Ga12 (X = Li~Kr) Clusters. *Crystals* **2022**, *12*, 543. [CrossRef]
9. Chiu, T.H.; Liao, J.-H.; Gam, F.; Chantrenne, I.; Kahlal, S.; Saillard, J.-Y.; Liu, C.W. Homoleptic Platinum/Silver Superatoms Protected by Dithiolates: Linear Assemblies of Two and Three Centered Icosahedra Isolobal to Ne_2 and I_3^-. *J. Am. Chem. Soc.* **2019**, *141*, 12957–12961. [PubMed]
10. Zhong, Y.-J.; Liao J-HChiu, T.-H.; Kahlal, S.; Lin C-JSaillard, J.-Y.; Liu, C.W. A Two-Electron Silver Superatom Isolated from Thermally Induced Internal Redox Reaction of A Silver(I) Hydride. *Angew. Chem. Int. Ed.* **2021**, *60*, 12712–12716. [CrossRef]
11. Sharma, S.; Chakrahari, K.-K.; Saillard, J.-Y.; Liu, C.W. Structurally Precise Dichalcogenolate-Protected Copper and Silver Superatomic Nanoclusters and Their Alloys. *Acc. Chem. Res.* **2018**, *51*, 2475–2483. [CrossRef]
12. Hirai, H.; Ito, S.; Takano, S.; Koiasu, K.; Tsukunda, T. Ligand-protected gold/silver superatoms: Current status and emerging trends. *Chem. Sci.* **2020**, *11*, 12233–12248. [PubMed]
13. de Heer, W.A. The physics of simple metal clusters: Experimental aspects and simple models. *Rev. Mod. Phys.* **1993**, *65*, 611–676.
14. Neukermans, S.; Janssens, E.; Chen, Z.F.; Silverans, R.E.; Schleyer, P.V.R.; Lievens, P. Extremely stable metal-encapsulated $AlPb_{10}^+$ and $AlPb_{12}^+$ Clusters: Mass-Spectrometric Discovery and Density Functional Theory Study. *Phys. Rev. Lett.* **2004**, *92*, 163401. [CrossRef]
15. Jahn, H.A.; Teller, E. Stability of polyatomic molecules in degenerate electronic states. I. Orbital degeneracy. *Proc. R. Soc. Lond. Ser. A-Math. Phys. Sci.* **1937**, *161*, 220–235.
16. Feynman, R.P.; Leighton, R.B.; Sands, M. *The Feynman Lectures on Physics*; Basic Books: New York, NY, USA, 2013; Volume III, pp. 3–34.
17. Jiang, D.; Kühn, M.; Tang, Q.; Weigend, F. Superatomic Orbitals under Spin-Orbit Coupling. *J. Phys. Chem. Lett.* **2014**, *5*, 3286–3289. [CrossRef]
18. Liu, X.; Bauer, M.; Bertagnolli, H.; Roduner, E.; van Slageren, J.; Phillipp, F. Structure and magnetization of small monodisperse platinum clusters. *Phys. Rev. Lett.* **2006**, *97*, 253401, Erratum in *Phys. Rev. Lett.* **2009**, *102*, 049902. [CrossRef] [PubMed]
19. Jensen, C.; Buck, D.; Dilger, H.; Bauer, M.; Phillipp, F.; Roduner, E. Maximum hydrogen chemisorption on KL zeolite supported Pt clusters. *Chem. Commun.* **2013**, *49*, 588–590. [CrossRef]

20. Keppeler, M.; Roduner, E. Platinum-hydrogen vibrations and low energy electronic excitations of 13-atom Pt nanoclusters. *Phys. Chem. Chem. Phys.* **2014**, *16*, 26613–26616. [CrossRef]
21. Roduner, E.; Jensen, C. Magnetic Properties and the Superatom Character of 13-Atom Platinum Nanoclusters. *Magnetochemistry* **2015**, *1*, 28–44. [CrossRef]
22. Bartolomé, J.; Bartolomé, F.; García, L.M.; Roduner, E.; Akdogan, Y.; Wilhelm, F.; Rogalev, A. Magnetization of Pt_{13} clusters supported in a NaY zeolite: A XANES and XMCD study. *Phys. Rev. B* **2009**, *80*, 014404. [CrossRef]
23. Jensen, C.; van Slageren, J.; Jakes, P.; Eichel, R.A.; Roduner, E. Support Effects on Hydrogen Desorption, Isotope Exchange, Chemical Reactivity, and Magnetism of Platinum Nanoclusters in KL Zeolite. *J. Phys. Chem. C* **2013**, *117*, 22732–22745.
24. Roduner, E.; Jensen, C.; van Slageren, J.; Rakoczy, R.A.; Larlus, O.; Hunger, M. Anomalous Diamagnetic Susceptibility in 13-Atom Platinum Nanocluster Superatoms. *Angew. Chem. Int. Ed.* **2014**, *53*, 4318–4321. [CrossRef] [PubMed]
25. Yamamoto, Y.; Miura, T.; Nakae, Y.; Teranishi, T.; Miyake, M.; Hori, H. Anomalous spin polarization in Pd and Au nano-particles. *Phys. B* **2003**, *329–333*, 1183. [CrossRef]
26. Yamamoto, Y.; Hori, H. Direct observation of the ferromagnetic spin polarization in gold nanoparticles, a review. *Rev. Adv. Mater. Sci.* **2006**, *12*, 23–32.
27. Dyrek, K.; Che, M. EPR as a Tool to Investigate the Transition Metal Chemistry on Oxide Surfaces. *Chem. Rev.* **1997**, *97*, 305–331. [CrossRef]
28. Desclaux, J.P. *Atomic Data and Nuclear Data Tables*; Elsevier: Amsterdam, The Netherlands, 1973; Volume 12, pp. 311–406.
29. Watari, N.; Ohnishi, S. Atomic and electronic structures of Pd_{13} and Pt_{13} clusters. *Phys. Rev. B Condens. Matter* **1998**, *58*, 1665–1677. [CrossRef]
30. Hammer, B.; Nørskov, J.K. Why gold is the noblest of all the metals. *Nature* **1995**, *376*, 238–240. [CrossRef]
31. Kresin, V. Electronic structure of small metal clusters: Thomas-Fermi statistical theory. *Phys. Rev. B* **1988**, *38*, 3741–3746.
32. Raju, Y.; Krishnamurthi, P.; Paulose, P.L.; Manoharan, P.T. Substrate-free copper nanoclusters exhibit super diamagnetism and surface based soft ferromagnetism. *Nanoscale* **2017**, *9*, 17963–17974. [CrossRef]
33. Nealon, G.L.; Donnio, B.; Greget, R.; Kappler, J.-P.; Terazzi, E.; Gallani, J.L. Magnetism in gold nanoparticles. *Nanoscale* **2012**, *4*, 5244–5258. [CrossRef]
34. Wu, M.; Kandalam, A.K.; Gutsev, G.L.; Jena, P. Origin of the anomalous magnetic behavior of the $Fe13^{+}$ cluster. *Phys. Rev. B* **2012**, *86*, 174410. [CrossRef]
35. Bergeron, D.E.; Castleman, W.; Morisato, T.; Khanna, S.N. Formation of $Al_{13}I^{-}$: Evidence for the Superhalogen Character of Al_{13}. *Science* **2004**, *304*, 84–87. [CrossRef] [PubMed]
36. Eremets, M.I.; Minkov, V.S.; Drozdov, A.P.; Kong, P.P.; Ksenofontov, V.; Shylin, S.I.; Bud'ko, S.L.; Prozorov, R.; Balakirev, F.F.; Sun, D.; et al. High-Temperature Superconductivity in Hydrides: Experimental Evidence and Details. *J. Supercond. Nov. Magn.* **2022**, *35*, 965–977.
37. Kresin, V.Z.; Ovchinnikov, Y.N. 'Giant' strengthening of superconducting pairing in metallic nanoclusters: Large enhancement of T_c and potential for room-temperature superconductivity. *Phys. Uspekhi* **2008**, *51*, 427–435.